International Journal of Modern Physics A
Vol. 36, Nos. 11 & 12 (2021) 2140019 (16 pages)

DOI: 10.1142/S0217751X21400194

The drag-free control design and in-orbit experimental results of "Taiji-1"

Zhiqiang Hu[*,‡‡], Pengcheng Wang[*,‡‡], Jianfeng Deng[*], Zhiming Cai[*,†], Zhi Wang[‖], Zuolei Wang[‡], Jinpei Yu[*], Yueliang Wu[*,§], Qi Kang[¶], Huawang Li[*,**,§§] and Yonghe Zhang[*,††,§§]

[*]*Innovation Academy for Microsatellites, Chinese Academy of Sciences, Shanghai, China*

[†]*Zhejiang University, Hangzhou, China*

[‡]*Lanzhou Institute of Space Technology Physics, Lanzhou, China*

[§]*Beijing Institute of Theoretical Physics, Chinese Academy of Science, Beijing, China*

[¶]*Institute of Mechanics, Chinese Academy of Science, Beijing, China*

[‖]*Changchun Institute of Optics, Fine Mechanics and Physics, Changchun, China*
[**]*lihw@microsate.com*
[††]*zhangyh@microsate.com*

[¶¶]*On behalf of The Taiji Scientific Collaboration*

Received 15 September 2020
Revised 16 October 2020
Accepted 30 October 2020
Published 6 April 2021

Taiji is China's spaceborne gravitational wave (GW) detecting project, which is designed to detect GW sources ranging from 0.1mHz to 1Hz. Taiji-1, launched on 31 August 2019, is a pilot study mission to prepare necessary technology for Taiji pathfinder. Two major technology units were tested on Taiji-1: Optical Metrology System and Drag-free Control System (DFCS). In this paper, we try to illustrate the design of DFCS; the implemenstation strategy of experiment and the first results of in-orbit experiment. The disturbance reduction capability of Taiji-1's DFCS is demonstrated by the in-orbit experimental performance analysis.

Keywords: Taiji-1; drag-free control; embedded model control; anti-aliasing filtering.

1. Introduction

Taiji is China's spaceborne GW detection mission proposed in 2008, which is designed to detect GW sources ranging from 0.1 mHz and 1 Hz. Taiji mission consists of three completely identical spacecrafts following a heliocentric orbit ahead or behind the Earth with the angle of 20°.[1,2] The three spacecrafts form a giant equilateral triangle with the arm length being approximately three million kilometers shown in Fig. 1. Each spacecraft

[‡‡]These authors contributed equally to this work.
[§§]Corresponding authors.
[¶¶]For more details, please refer to article 2102002 of this Special Issue.

Fig. 1. Taiji's orbit and configuration.

carries a pair of lasers ranging interferometers and two gravitational reference sensors (GRS), working as the reflective surface of laser with the other two forming three Michelson-type interferometers. The DFCS offers an ultra-stable spacecraft platform and a sub-femto-g inertial reference for laser ranging interferometer within the measurement frequency band. The laser interferometer needs to reach pico-meter precision to detect weak GW signals.

Based on the study of preliminary scientific goals and key technology research, Taiji team decides to take three steps launching last three satellites to detect GW.[3] The first step is to launch a satellite called Taiji-1 in 2019, which is a pilot study mission to prepare necessary technology for Taiji pathfinder (the second step). Taiji pathfinder (Taiji-2) consisting of two spacecrafts will be used to demonstrate Taiji technology around 2023–2025, probably working as a heliocentric orbital mission. As a pilot study mission, Taiji-1 needs to explore the manufacturing process and in-orbit working sequence for Taiji payload; practice the data processing stream for Taiji mission and verify the feasibility of some Taiji key technologies in space.

Approved by the Chinese Academy of Sciences (CAS) on 30 August 2018 and launched on 31 August 2019, Taiji-1 is a smooth mission. The orbit of Taiji-1 was a 600km circular dawn/dusk Sun-synchronous orbit inclined 97.69°. Two major technology units onboard Taiji-1 were tested: Optical Metrology System (OMS)[4] and Drag-free Control System (DFCS).[5] With the short-term development cycle and limited budget, the payload design was highly simplified. OMS consists of optical bench, phasemeter and two laser sources, while DFCS is composed of GRS, drag-free controller and two μN-thrusters (Radio frequency ion thruster and Hall effect thruster). Figure 2 shows how the payload distributed on Taiji-1.[3]

This paper mainly introduces the design of drag-free control and Taiji-1's in-orbit experiment results. Taiji-1 functions well and has finished its in-orbit testing phase on 25 December 2019. The satellite has started the task extending phase after completing its set goals.

Next chapters are organized as follows:

- Section 2 illustrates the method to design and develop the controller;
- Section 3 analyzes the mathematic simulations;
- Section 4 describes the process of experiment;

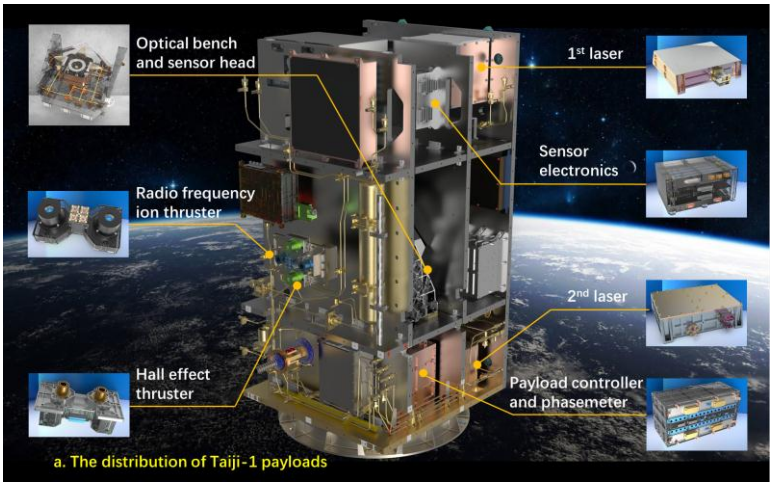

Fig. 2. The configuration of Taiji-1 with payloads.

- Section 5 explains in-orbit experiment results.
- Section 6 concludes

2. Drag-Free Control Concept

The principle of DFCS is to place a metal mass called test mass (TM) in the center of the satellite and isolate it from the external nongravitational force perturbations. The change of distance or acceleration of TM relative to the satellite is measured by the principle of capacitive sensing or laser interference. The DFCS adjusts the thrust to offset external non-conservative force according to measured signals, so that the satellite can always track TM flight. The control function that uses the relative distance as feedback is called the displacement mode drag-free control. This mode is often used for the laser link measurement direction (sensitive axis direction) during gravitational wave (GW) detection. The acceleration mode DFC that uses relative acceleration changes as feedback is called acceleration drag-free control, which is often used for gravity field measurement satellites. This paper mainly introduces DFCS's acceleration mode and Taiji-1's in-orbit experiment results.[6,7]

In recent years, the embedded model control (EMC), a kind of model-based control strategy, was proposed and applied to the disturbance rejection control tasks. The embedded model (EM) is constructed for the plant's controllable dynamics, the disturbance dynamics and the neglected part of the control loop. Combining measurements and EM outputs, the disturbance is estimated and then is rejected by the control output.[8] The DFC operation in LEO is a typical disturbances rejection task. The EMC approach has been designed and simulated for the DFC, the attitude control and the formation control. The theoretical analysis and simulation results demonstrated the effectiveness of this methodology.[9–11] For the Taiji-1 DFC task, the EMC method is utilized following the work of Ref. 8.

The disturbance reduction function of the acceleration mode drag-free control is highly constrained by sensors and actuators dynamics. The EMC theory is used to construct the drag-free controller in the project.

2.1. *The embedded model*

The embedded model (EM) can be described as follows

$$\left.\begin{aligned} &\boldsymbol{x}(i+1)=\boldsymbol{A}\boldsymbol{x}(i)+\boldsymbol{B}\boldsymbol{u}(i)+\boldsymbol{G}\boldsymbol{w}(i)\\ &\boldsymbol{x}(0)=0\\ &\boldsymbol{y}_m=\boldsymbol{C}\boldsymbol{x}(i),\boldsymbol{z}_m(i+1)=\boldsymbol{F}\boldsymbol{x}(i) \end{aligned}\right\} \tag{1}$$

with,

$$\boldsymbol{x}=\begin{bmatrix}\boldsymbol{x}_c\\ \boldsymbol{x}_d\end{bmatrix},\quad \boldsymbol{A}=\begin{bmatrix}\boldsymbol{A}_c & \boldsymbol{H}_c\\ \boldsymbol{0} & \boldsymbol{A}_d\end{bmatrix},\quad \boldsymbol{B}=\begin{bmatrix}\boldsymbol{B}_c\\ \boldsymbol{0}\end{bmatrix},\quad \boldsymbol{C}=\begin{bmatrix}\boldsymbol{C}_c & \boldsymbol{C}_d\end{bmatrix},\quad \boldsymbol{F}=\begin{bmatrix}\boldsymbol{F}_c & \boldsymbol{0}\end{bmatrix}.$$

$\boldsymbol{x}_c$ is the controllable state, and $\boldsymbol{x}_d$ is the disturbance state, the pairs of $(\boldsymbol{A}_c,\boldsymbol{B}_c)$ and $(\boldsymbol{A},\boldsymbol{G})$ are assumed to be controllable, while the pairs $(\boldsymbol{F}_c,\boldsymbol{A}_c)$ and $(\boldsymbol{C},\boldsymbol{A})$ are assumed to be observable. The relative acceleration between TM and satellite is modeled as:

$$\boldsymbol{A}_{sm}=\boldsymbol{f}_{ng}+\boldsymbol{f}_c+\boldsymbol{g}_g+\dot{\boldsymbol{\omega}}\times\boldsymbol{d}+\boldsymbol{\omega}\times(\boldsymbol{\omega}\times\boldsymbol{d})+\ddot{\boldsymbol{d}}+2\boldsymbol{\omega}\times\dot{\boldsymbol{d}}+\mathbf{w}_d \tag{2}$$

$\boldsymbol{f}_{ng}$ is the nongravitational acceleration caused by external disturbance, $\boldsymbol{f}_c$ is the compensation acceleration generated by the thruster, $\boldsymbol{g}_g$ is the gravity gradient caused by the satellite, $\boldsymbol{\omega}$ and $\dot{\boldsymbol{\omega}}$ is the angular velocity and angular acceleration of the satellite, $\boldsymbol{d}$ is the distance between the center of mass of the TM and satellite, and $\mathbf{w}_d$ is the unmodeled acceleration.

Because the zero-relative acceleration between TM and the satellite along the z_b direction is the control purpose in Taiji-1's task, the model output and performance output are the same and built as follows

$$y_m=z_m=\boldsymbol{A}_{sm}(3) \tag{3}$$

with $\boldsymbol{A}_{sm}(3)$ is the third component of the $\boldsymbol{A}_{sm}$ in z-axis,

$$\begin{aligned} &A_c=0,\quad \boldsymbol{H}_c=\begin{bmatrix}1 & 0\end{bmatrix},\quad \boldsymbol{A}_d=\begin{bmatrix}1 & 1\\ 0 & 1\end{bmatrix},\quad B_c=1,\quad \boldsymbol{G}_c=\begin{bmatrix}1 & 0 & 0\end{bmatrix}\\ &\boldsymbol{G}_d=\begin{bmatrix}0 & 1 & 0\\ 0 & 0 & 1\end{bmatrix},\quad G_c=1,\quad \boldsymbol{C}_d=\begin{bmatrix}0 & 0\end{bmatrix},\quad F_c=1 \end{aligned} \tag{4}$$

after the Z-transformation, the counterpart of the actual output dynamic y has the following manner

$$y(z)=\boldsymbol{P}(z)u(z)+\upsilon_y(z) \tag{5}$$

$\boldsymbol{P}(z)$ is related to the measurement characteristics of GRS, the thrust noise of the μN-thrusters and the time delay. υ_y represents the influence of the unknown disturbance and noise.

EM can be divided into two parts, one part is controllable, which is called the reference dynamic shown as

$$\left.\begin{aligned} &\underline{x}(i+1) = A_c\underline{x}(i) + B_c\underline{u}(i) \\ &\underline{x}(0) = \underline{x}_0 \\ &\underline{z}(i) = F_c\underline{x}(i), \underline{z}(z) = M(z)\underline{u}(z) \end{aligned}\right\} \tag{6}$$

The other part is uncontrollable, called disturbance dynamics

$$\left.\begin{aligned} &\boldsymbol{x}_d(i+1) = \boldsymbol{A}_d\boldsymbol{x}_d(i) + \boldsymbol{G}_d\boldsymbol{w}(i) \\ &\boldsymbol{d}(i) = \boldsymbol{H}_c\boldsymbol{x}_d(i) + \boldsymbol{G}_c\boldsymbol{w}(i) \\ &\boldsymbol{x}_d(0) = 0 \end{aligned}\right\} \tag{7}$$

The reference model describes the desired reference trajectory. For acceleration mode DFC, the desired relative acceleration of the satellite body w.r.t. TM is zero. The disturbance model is introduced to describe the disturbance including the environmental disturbance, the thrust disturbance and the dynamics of measured acceleration changes caused by the satellite's attitude movement.

2.2. *The control requirements*

The performance indicator of the reference model is $\underline{z}$, when there is no external disturbance, otherwise, the performance indicator is z_m. Since the external disturbance could change the reference trajectory, the error can be described as

$$\underline{e} = \underline{z} - z_m = \underline{y} - y_m \tag{8}$$

The aim of the DFC is to make the performance index status z_m as close as possible to the expected reference performance index status $\underline{Z}$, in the presence of unknown external perturbation. In order to meet the control accuracy index, the error should meet the following requirement

$$\|\underline{e}\| \le \varepsilon(\underline{z}) \tag{9}$$

$\varepsilon(\underline{z})$ is the control demand boundary.

2.3. *Noise estimator*

A noise estimator is adopted to estimate the external nongravitational force acceleration. The detail of the design of estimator can refer to Ref. 8.

$$\bar{\boldsymbol{w}}(z) = \boldsymbol{L}(z)\bar{\boldsymbol{e}}(z) = \boldsymbol{L}(z)\left(\boldsymbol{y}(z) - \hat{\boldsymbol{y}}_m(z)\right) \tag{10}$$

Here, $\boldsymbol{L}(z)=\boldsymbol{L}_d(z)+\boldsymbol{L}_w(z)$, the definition of each parameter is the same as that in reference.

2.4. *Error loop stability and performance*

Based on the conclusion in Ref. 8, we can learn the condition of the stability of the control error loop

$$\max_{|f|\le f_{\max}}\left|\left(\boldsymbol{V}_m\left(e^{j2\pi fT}\right)-\boldsymbol{S}_w\left(e^{j2\pi fT}\right)\right)\partial\boldsymbol{P}\left(e^{j2\pi fT};\boldsymbol{p}\right)\right|\le\eta\le 1 \tag{11}$$

with,

$$\boldsymbol{S}_w=\boldsymbol{S}_c\boldsymbol{M}\boldsymbol{N}\boldsymbol{L}_w\boldsymbol{S}_m,\quad \boldsymbol{S}_c=\left(1+\boldsymbol{T}\boldsymbol{M}\right)^{-1},\quad \boldsymbol{T}\boldsymbol{M}=\boldsymbol{K}\left(z\boldsymbol{I}-\boldsymbol{A}_c\right)^{-1}\boldsymbol{B}_c$$
$$\boldsymbol{V}_m=\frac{\boldsymbol{M}\left(\boldsymbol{D}\boldsymbol{L}_d+\boldsymbol{N}\boldsymbol{L}_w\right)}{1+\boldsymbol{M}\left(\boldsymbol{D}\boldsymbol{L}_d+\boldsymbol{N}\boldsymbol{L}_w\right)},\quad \partial\boldsymbol{P}=\boldsymbol{P}\boldsymbol{M}^{-1}-1 .$$

The error loop $\underline{\boldsymbol{e}}$ can be rewritten as

$$\left\|\underline{\boldsymbol{e}}\right\|=\left\|\left(1+\left(\boldsymbol{V}_m-\boldsymbol{S}_w\right)\partial\boldsymbol{P}\right)^{-1}\left(\boldsymbol{V}_m-\boldsymbol{S}_w\right)\left(\partial\boldsymbol{P}\underline{y}+v_e\right)\right\|\le\varepsilon\left(\underline{y}\right) \tag{12}$$

For the desired reference trajectory, $\underline{y}=0$, then

$$\begin{aligned}\left\|\underline{\boldsymbol{e}}\right\|&=\left\|\left(1+\left(\boldsymbol{V}_m-\boldsymbol{S}_w\right)\partial\boldsymbol{P}\right)^{-1}\left(\boldsymbol{V}_m-\boldsymbol{S}_w\right)\left(v-\left(\boldsymbol{V}_m-\boldsymbol{S}_w\right)^{-1}\left(\boldsymbol{S}_m-\boldsymbol{S}_w\right)\boldsymbol{M}\left(d_u-w_u\right)\right)\right\|\\&=\left\|\left(1+\left(\boldsymbol{V}_m-\boldsymbol{S}_w\right)\partial\boldsymbol{P}\right)^{-1}\left(\boldsymbol{V}_m-\boldsymbol{S}_w\right)v-\left(1+\left(\boldsymbol{V}_m-\boldsymbol{S}_w\right)\partial\boldsymbol{P}\right)^{-1}\left(\left(\boldsymbol{S}_m-\boldsymbol{S}_w\right)\boldsymbol{M}\left(d_u-w_u\right)\right)\right\|,\end{aligned} \tag{13}$$

where, v represents the measurement noise and constant bias of GRS, d_u characterizes external nongravitational interference, thrust noise and coupling interference caused by installation errors with other axes.

The above formula can be written in the form of power spectral density (PSD) as

$$\underline{S}_e(f)=\sqrt{\begin{aligned}&\left|\left(1+\left(\boldsymbol{V}_m-\boldsymbol{S}_w\right)\partial\boldsymbol{P}\right)^{-1}\left(\boldsymbol{V}_m-\boldsymbol{S}_w\right)\right|^2 S_v^2(f)+\\&\left|\left(1+\left(\boldsymbol{V}_m-\boldsymbol{S}_w\right)\partial\boldsymbol{P}\right)^{-1}\left(\left(\boldsymbol{S}_m-\boldsymbol{S}_w\right)\boldsymbol{M}\right)\right|^2\left(S_d^2(f)+S_w^2(f)\right)\end{aligned}}\le\underline{S}_{e,\max}(f), \tag{14}$$

where, S_v, S_d, S_w are the ASD of v, d_u, w_u respectively. $\underline{S}_e(f)$ is the ASD of the residual acceleration measured by GRS after acceleration drag-free control.

The transfer function of the external disturbance x_d to the output of GRS (the suppression ability of the drag control to the external disturbance and thrust noise) can be derived

$$P_{DF}=\left(1+\left(V_m-S_w\right)\partial P\right)^{-1}\left(S_m+S_w\right)M \tag{15}$$

The transfer function of the measurement noise and constant bias to the output of GRS (the suppression ability of the drag control to the measurement noise and constant bias) can be derived

$$P_V = \left(1+\left(V_m - S_w\right)\partial P\right)^{-1}\left(V_m - S_w\right) \tag{16}$$

3. Theoretical Performance Analysis

In the simulation, the transfer function of GRS is supposed to

$$P_{GRS} = \frac{36s^2 + 103.7s + 298.6}{5.53e^{-4}s^4 + 0.347s^3 + 36s^2 + 97.21s + 298.6}. \tag{17}$$

The uncertainty of the calibration coefficient of GRS $\partial b = 0.05$, the closed-loop time delay is supposed to 115 ms. The parameter of the noise estimator is $\boldsymbol{L} = \begin{bmatrix} 3\lambda - 1 & 3\lambda^2 & \lambda^3 \end{bmatrix}^T$, here, $1-\lambda$ is the eigenvalues of the matrix of $[A\text{-}GLC]$.

Two kinds of thrusters with different characteristics are used to evaluate the performance of drag-free control based on the above analysis. One with long thrust command delay and response time, the other with short command delay and response time, and the transfer functions of the two thrusters are

$$P_{t1} = \frac{80.9294e^{-0.16875s}}{s^2 + 17.9699s + 80.9294}, \tag{18}$$

$$P_{t2} = \frac{1129.971e^{-0.009s}}{s^2 + 67.23s + 1129.971}. \tag{19}$$

The simulation results are shown in Figs. 3–8.

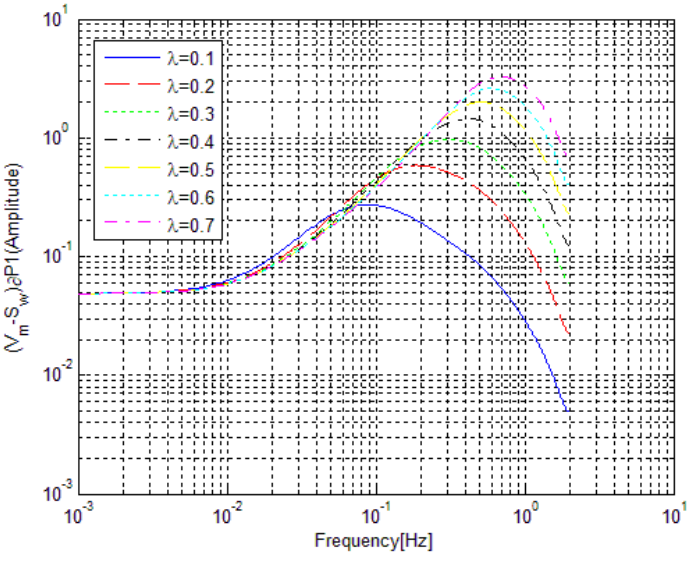

Fig. 3. The loop gain $((V_m - S_w)\partial P)$ of the thruster 1 with different λ.

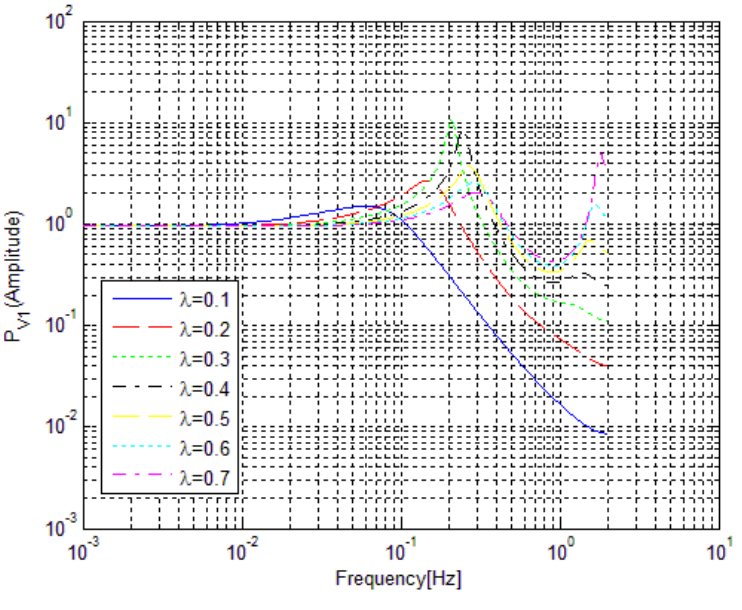

Fig. 4. The suppression ability P_V of the thruster 1 with different λ.

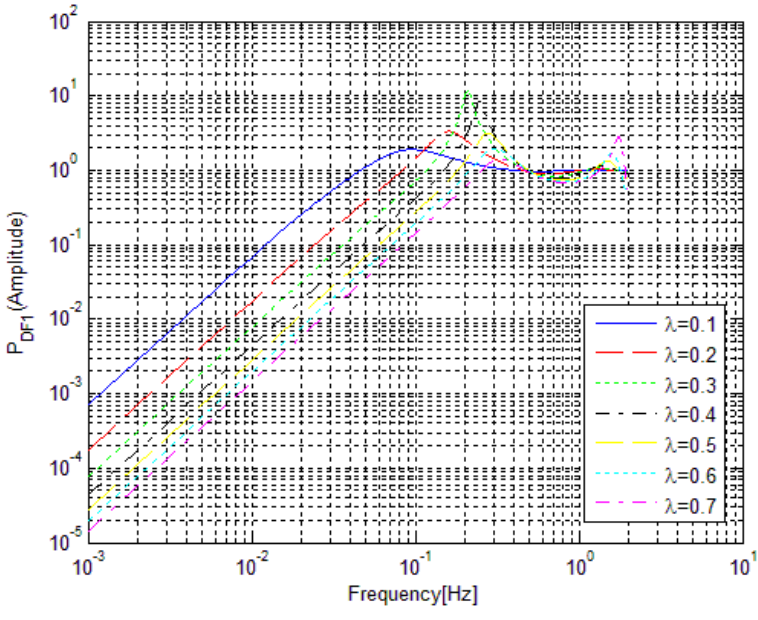

Fig. 5. The suppression ability P_{DF} of the thruster 1 with different λ.

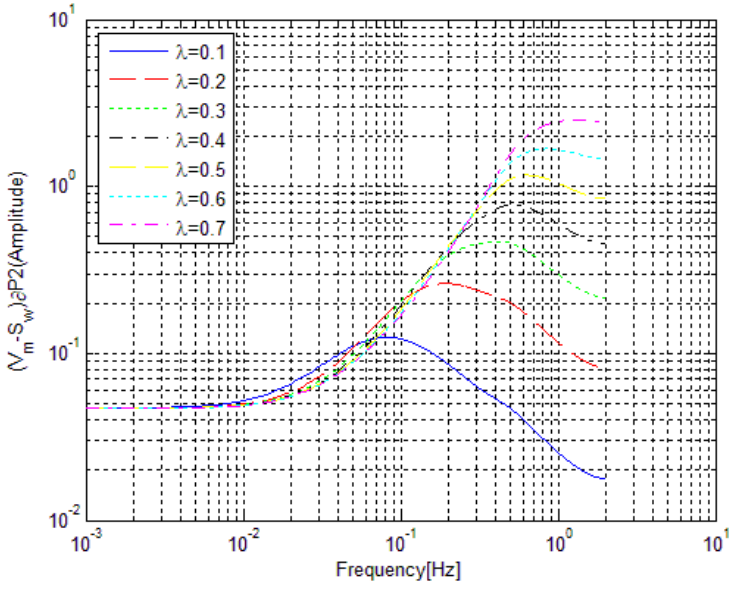

Fig. 6. The loop gain $((V_m - S_w)\partial P)$ of the thruster 2 with different λ.

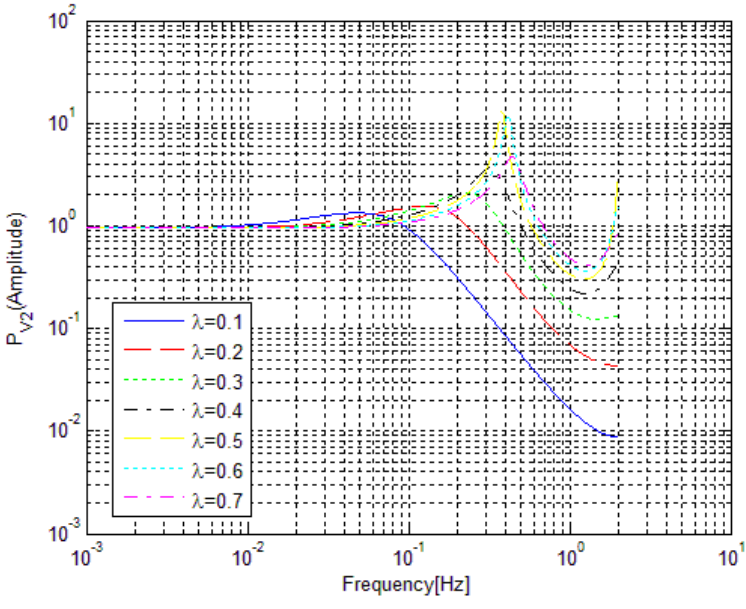

Fig. 7. The suppression ability P_V of the thruster 2 with different λ.

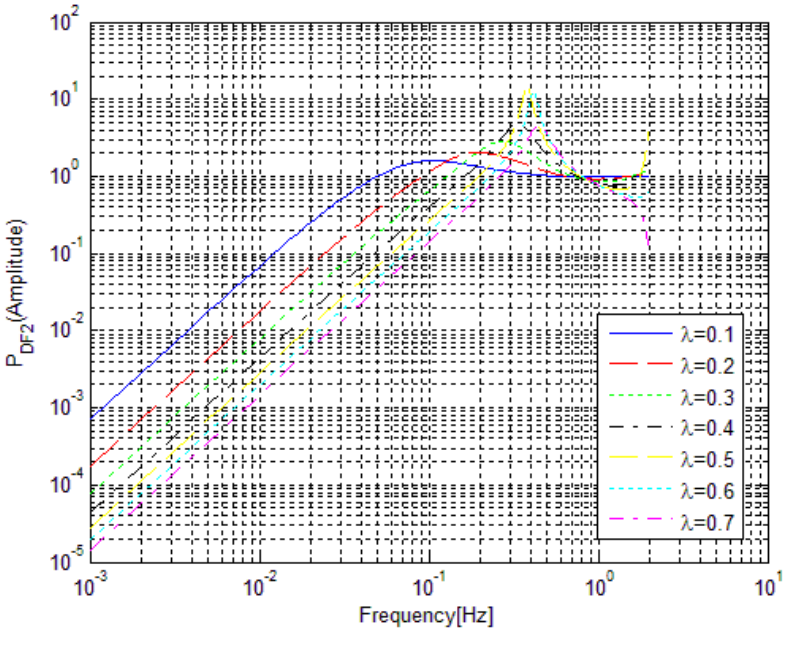

Fig. 8. The suppression ability P_{DF} of the thruster 2 with different λ.

From the simulation, we can conclude:

(1) With the external disturbance above 0.1Hz, the larger the value λ, the stronger the suppression ability, the suppression ability is not obvious above 0.1Hz.
(2) With the same λ below 0.1Hz, the greater the thrust delay and slower the response of the thruster, the more obvious amplification of the measurement noise and constant bias, and the poor performance of the drag-free control.
(3) The parameter of λ should be determined with the total bandwidth 0.01–1Hz. In addition, based on the above analysis, instructing us to select parameter λ. We also have analyzed and compared the influence of transfer functions with different inertial sensors on the drag-free control performance, which will not be repeated here.

4. Design of the Drag-Free Control Experiment

Taiji-1 is a ground-orientation satellite in normal mode with +z pointing to Earth, the μN-thrusters and sensitive axis of GRS are installed along with *z*-axis of the satellite. For DFCS in-orbit testing, the specific implementation scheme of in-orbit drag-free control experiment can be described as follows:

Step 1. An active disturbance is generated by the thruster (+z direction) with the following form:

$$F_{+z} = A_1 \sin\left(2\pi f_1 t + \varphi_1\right) + B_1 \tag{20}$$

where, $f_1 \in [0.01 \quad 1]$Hz , and $B_1 > A_1$ in order to ensure the thruster is out of dead zone and the symbol of the thrust will not change.

Step 2. Before drag-free control experiment, a disturbance is generated by the thruster when the satellite is free floating (all the actuator is shut down).

Step 3. The GRS constant bias can be calibrated by the experiment data from step 2 and uploaded to the drag-free controller.

Step 4. The drag-free control experiment is conducted with the same orbit environment as step 1 in order to reduce effect of the unknown disturbance. The controller generates the control order with the updated GRS constant bias and its measurement, and output to the thrusters installed in -z face to offset the active disturbance, and

$$F_{-z} = F_{df} \tag{21}$$

Step 5. The performance of the drag-free control can be concluded from comparison of the results from step 2 to step 4.

Step 6. Repeat step 1 to step 5.

5. In-Orbit Experimental Results

Before in-orbit drag-free control, we calibrate the constant bias of GRS, the noise of the thruster, and so on. During the experiment, we find that the high-frequency measurement

noise will affect the performance of experiment. So, an anti-aliasing filter is adopted to pre-process the measurement data of GRS, and the parameter of controller is revised correspondingly.

5.1. *Anti-aliasing filter for the GRS outputs*

In the acceleration control mode, an anti-aliasing filter is designed and introduced into the control loop. The raw GRS acceleration measurement at 100Hz sampling frequency can be used for the acceleration mode drag-free control. This acceleration measurement has to be down-sampled at 4Hz as the control unit input.

From in-orbit testing results, without the control and injected disturbance, the acceleration measurement amplitude spectral density (ASD) spectrum along the earth center direction is nearly flat and around $8\times10^{-9}\,\mathrm{m/s^2/Hz^{0.5}}$ in the bandwidth 1mHz–50Hz. Based on the orbit environment and platform-GRS performance analysis, the GRS internal capacitive sensor/control noise is considered to dominate this GRS readout ASD.

After the down-sampling, the higher frequency measurement noise would raise the lower bandwidth noise ASD significantly. In order to avoid this aliasing influence, an anti-aliasing filter is introduced and fed with the 100Hz raw measurement. This anti-aliasing filter is designed as a 28-order FIR low-pass filter, which can reduce the higher frequency part (>2Hz) of the GRS raw 100Hz readout. (The designed magnitude

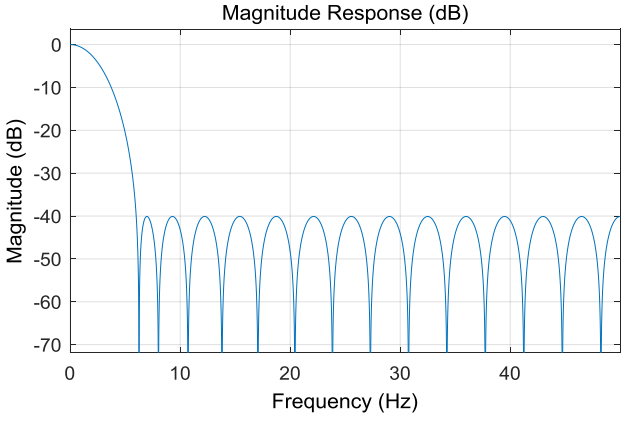

Fig. 9. Magnitude response of the anti-aliasing filter.

responds of the filter is shown in the following figure.) The filtered and down-sampled 4Hz measurement is used for the DFCS computer directly. The time delay resulting from this anti-aliasing filter is about 0.15s.

From the in-orbit testing data processing, without acceleration mode drag-free control, the ASD of the 100Hz raw measurements is almost as same as that of the filtered and down-sampled 4Hz readout under 2Hz, that means this filter is suitable for DFCS.

5.2. *In-orbit DFC performance*

In Taiji-1's acceleration mode drag-free control, based on the filtered GRS measurements and RIT actuator onboard force calculation, the satellite's residual acceleration and DFC performance can be evaluated. The filtered GRS measurements are 100Hz signals, which are GRS 100Hz raw measurements readout filtered by the aforementioned anti-aliasing filter. As shown in Fig. 9, this filter cannot change ASD of the raw measurements at the lower bandwidth at most. The RITs force estimation provides a kind of high precision real thruster force estimation, which is the particular capability of RITs. According to the existing drag-free control results of other missions, the external environmental force perturbation along the earth-center direction on the Taiji-1 orbit is not significant comparing with micro-thruster force. That is, in the disturbance injection and DFCS operations, the sum of micro-thruster's force estimation divided by the satellite mass could be another observation of the residual acceleration besides the GRS measurement. The first set of experiments is conducted for testing the disturbance reduction capability at 0.05Hz. The ASD spectrums of GRS measurements under the disturbance injection and the DFCS operation are calculated and shown in Fig. 10, respectively. Without drag-free control, the acceleration ASD peak at 0.05Hz is 1.45×10^{-7} resulting from the injected sinusoidal disturbance. Under DFC, the ASD peak at 0.05Hz is reduced to 1.27×10^{-8}, which is lower than 10% of the former. At the frequency band of 0.03–0.3 Hz, the spectrum is flat and the value is around 7.5×10^{-8}, as similar as the

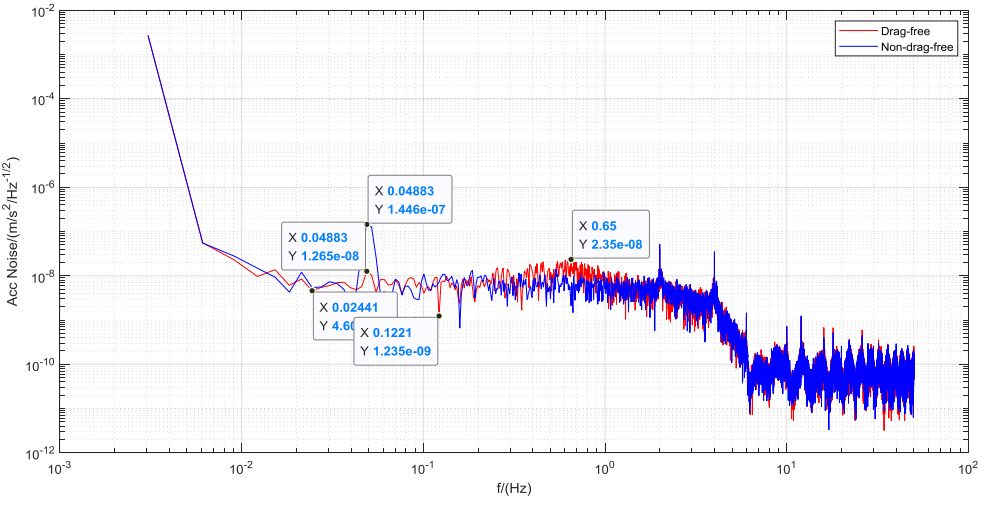

Fig. 10. (Color online) ASD spectrum of the GRS acceleration measurements along the earth-center direction under 0.05Hz disturbance with and without drag-free control (blue line: only disturbance injection; red line: disturbance injection and drag-free control).

disturbance injection case. Above 0.3Hz, the acceleration ASD under drag-free control is enlarged and reaches to 200% (around 0.7Hz). The GRS measurements are also plotted directly in Fig. 11. Without applying drag-free control, the sinusoidal injected disturbance acceleration is obvious. And using DFCS, that is attenuated. Additionally, because of the bias of the injected disturbance, the mean values of these two curves are not the same. In the 10mins without control testing, the acceleration readout has a small drifting. But with DFCS, the drifting is not observed, due to complementation capability of the controller. Under the same condition, the disturbance injection and DFCS operation has been repeated several times. The ASD spectrum results are almost the same. In some tests, the ASD under control is observed lower than that without drag-free control in band of 0.03–0.3Hz. The second experiment set is about the same amplitude sinusoidal at 0.07Hz. The results are demonstrated in the Figs. 12 and 13. As shown in Fig. 12, the ASD peak value at 0.07Hz is reduced near 75%, from 1.66×10^{-7} to 3.70×10^{-8}. Except the part around 0.07Hz, the ASD values in other bands are similar as those of 0.05Hz disturbance cases. And after applying drag-free control, the ASD of GRS measure is reduced nearly in the whole band of 0.03–0.3Hz. The GRS measurements curves are also similar as those under the 0.05Hz disturbance.

From these two sets experiments performances, the disturbance reduction capability of the Taiji-1 DFCS is demonstrated. Considering the readout noise of the GRS, the disturbance reducing effect is over 90% at 0.05Hz and over 80% at 0.07Hz. Obviously, the middle band of the real control system can cover the frequency point 0.07Hz. Based on the theoretical analyses, the mode of the sensitivity function can depict the external

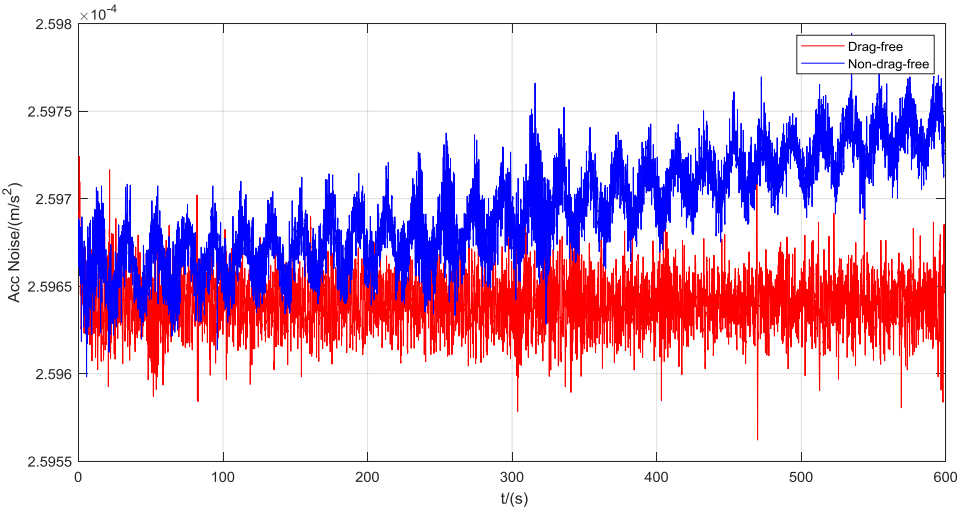

Fig. 11. (Color online) GRS acceleration measurements along the earth-center direction under 0.05Hz disturbance with and without drag-free control (blue line: only disturbance injection; red line: disturbance injection and drag-free control.)

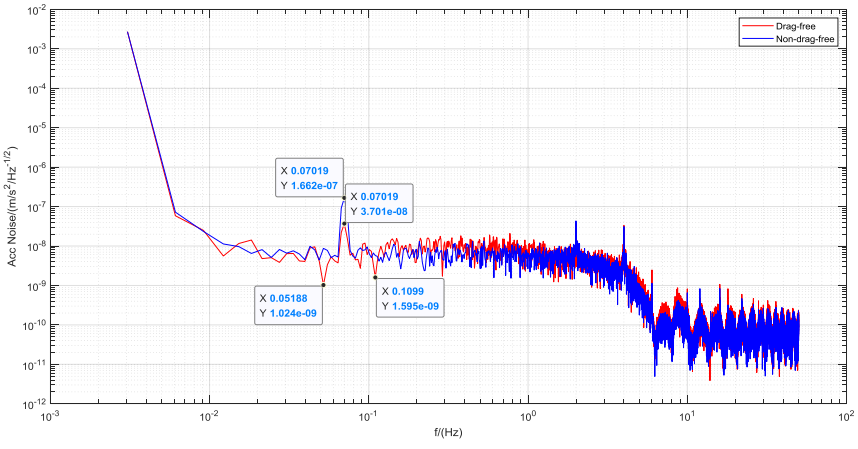

Fig. 12. (Color online) ASD spectrums of the GRS acceleration measurements along the earth-center direction under 0.07Hz disturbance with and without drag-free control (blue line: only disturbance injection; red line: disturbance injection and drag-free control).

perturbation reduction, and this function of EMC should have a slope of 40dB/dec, which coincides with the experimental observation. (The frequency raises nearly $2^{0.5}$, from 0.05Hz to 0.07Hz; the sensitivity function mode raises about 100%, from 10% to 20%). The enlarging effect over 0.3Hz could result from the complementary sensitivity peak.

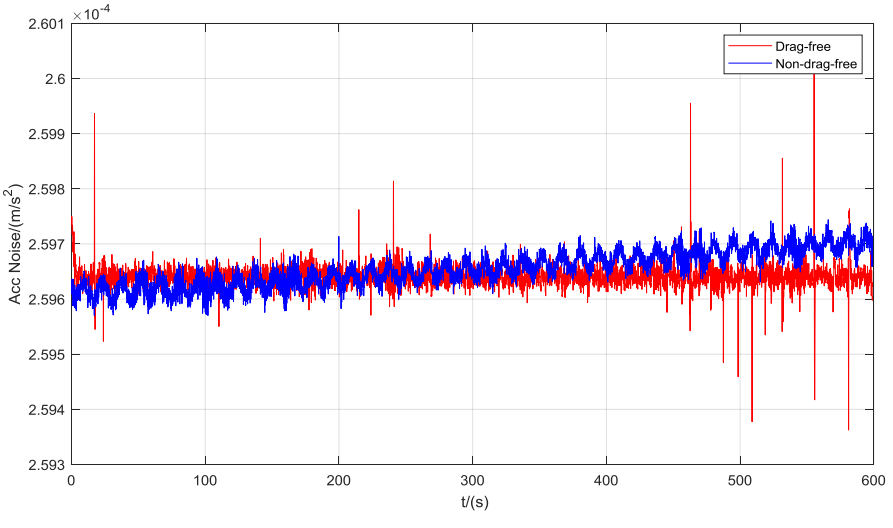

Fig. 13. (Color online) GRS acceleration measurements along the earth-center direction under 0.07Hz disturbance with and without drag-free control (blue line: only disturbance injection; red line: disturbance injection and drag-free control.)

The GRS sensing noise is enlarged. From these observed properties, the sensitivity function bandwidth could cover 0.1Hz. That is, the DFCS has the reduction capability for the disturbance below 0.1Hz. And from the on-orbit tests, the closed-loop time delay is estimated about 0.25s, near the system control period, including the GRS sensor, anti-aliasing filter, control unit and the RIT's response. The reduction effect is also observed in the frequency band of 0.03–0.1Hz, beside the injected disturbance frequency point. However, this reduction effect is not significant in the experimental observation.

In the following experiments, more testing will be conducted to test the DFCS properties. And then, the controller will be tuned to achieve more disturbance reduction capability.

6. Conclusion

The DFCS of Taiji-1 consists of the micro-Newton thruster (RIT and Hall effect thruster), GRS, anti-aliasing filter, and the controller. These dynamic models are constructed based on the ground test and modified according to the on-orbit calibration. A kind of disturbance observation and complementation method (EMC) is used for the Taiji-1 acceleration mode drag-free control. The control parameters are designed based on the theoretical analysis and simulation, and tuned in the on-orbit experiments. Several sets of experiments are conducted for the DFCS properties testing. The DFCS on-orbit performances are demonstrated and discussed. The disturbance reduction capability of the Taiji-1 DFCS is shown. The control system is planned to modify, and more on-orbit testing will be conducted in the near future.

Acknowledgments

This work is supported by the "Strategic Priority Research Program of the Chinese Academy of Science" (XDA15020705, XDA15020706, XDA15020707).

References

1. Z. R. Luo *et al*., *Prog. Theor. Exp. Phys.* ptaa083 (2020).
2. Z. R. Luo *et al*., *Results Phys.* **16**, 102918 (2019).
3. The Taiji Scientific Collaboration, Communications Physics, Probing the expanding gravitational universe and the nature of gravity with space borne gravitational wave antenna and the first step of China's efforts (to be printed) (2020).
4. H. E. Audley and the LISA Pathfinder collaboration, *J. Phys. Conf. Ser.* **840**, 012034 (2017).
5. W. Fichter *et al*., *Class. Quant. Grav.* **22**, S139 (2005).
6. J. F. Deng, Z. M. Cai, K. Chen *et al.*, *Chin. Optics* **012**, 503 (2019).
7. G. Sechi, M. Buonocore, F. Cometto *et al*., In-flight results from the drag-free and attitude control of goce satellite, in *IFAC Proc* (2011).
8. E. Canuto, *ISA Trans.* **46**, 363 (2007).
9. E. Canuto, A. Molano and L. Massotti, *IEEE Trans. Control Syst. Technol.* **18**, 501 (2010).
10. E. Canuto, A. Molano and C. Perez, *Acta Astronaut.* **72**, 121 (2012).
11. E. Canuto, A. Molano, C. Perez and L. Massotti, *Acta Astronaut.* **69**, 571 (2001).